Shock interactions, turbulence and the origin of the stellar mass spectrum

Ralph E. Pudritz and N. K.-R. Kevlahan

References	**This article cites 65 articles, 1 of which can be accessed free** http://rsta.royalsocietypublishing.org/content/371/2003/201202 48.full.html#ref-list-1
Subject collections	Articles on similar topics can be found in the following collections astrophysics (59 articles) interstellar medium (18 articles) stars (24 articles)
Email alerting service	Receive free email alerts when new articles cite this article - sign up in the box at the top right-hand corner of the article or click **here**

To subscribe to *Phil. Trans. R. Soc. A* go to:
http://rsta.royalsocietypublishing.org/subscriptions

PHILOSOPHICAL TRANSACTIONS OF THE ROYAL SOCIETY A

Review

CrossMark
click for updates

One contribution of 13 to a Theme Issue 'Turbulent mixing and beyond: non-equilibrium processes from atomistic to astrophysical scales II'.

Author for correspondence:
Ralph E. Pudritz
e-mail: pudritz@physics.mcmaster.ca

Shock interactions, turbulence and the origin of the stellar mass spectrum

Ralph E. Pudritz and N. K.-R. Kevlahan

Origins Institute, McMaster University, Hamilton, Ontario, Canada L8S 4M1

Supersonic turbulence is an essential element in understanding how structure within interstellar gas is created and shaped. In the context of star formation, many computational studies show that the mass spectrum of density and velocity fluctuations within dense clouds, as well as the distribution of their angular momenta, trace their origin to the statistical and physical properties of gas that is lashed with shock waves. In this paper, we review the observations, simulations and theories of how turbulent-like processes can account for the structures we see in molecular clouds. We then compare traditional ideas of supersonic turbulence with a simpler physical model involving the effects of multiple shock waves and their interactions in the interstellar medium. Planar intersecting shock waves produce dense filaments and generate vortex sheets that are essential to create the broad range of density and velocity structure in clouds. As an example, the lower-mass behaviour of the stellar initial mass function can be traced to the tendency of a collection of shock waves to build up a lognormal density distribution (or column density). Vorticity—which is essential to produce velocity structure over a very broad range of length scales in shocked clouds—can also be generated by the passage of curved shocks or intersecting planar shocks through such media. Two major additional physical forces affect the structure of star-forming gas—gravity and feedback processes from young stars. Both of these can produce power-law tails at the high-mass end of the initial mass function.

1. Overview: from gas to stars

The origin of stars in galaxies is directly coupled to the dynamics and structure of their interstellar gas.

What physical processes are responsible for converting gas, that is, in its most diffuse form, non-self-gravitating, into a stellar mass spectrum (known as the initial mass function, IMF) with a well-defined, possibly universal, simple form? Both the diffuse (atomic and ionized) and molecular gas components of the interstellar medium (ISM) have highly supersonic velocity dispersions indicating that shocks are ubiquitous. The propagation and collision of shock waves play an important role in the chain of events leading to star formation by compressing gas: pushing it into ever denser physical states that allow it to cool and fragment more efficiently. This process also sweeps material into a network of dense filaments. Both the compression and filamentary structure of over-dense regions help set up the conditions necessary for gravity to act. Molecular clouds are sufficiently cold and dense that gravitational forces are a major factor in the evolution of the densest regions. On small enough scales within such clouds (typically approx. 1 pc) in which star clusters are observed to form, gravity dominates and star formation occurs in the many dense gaseous 'cores' that are evident in cluster-forming regions. Filamentary structure has always been apparent in observations of the ISM [1], but the high-resolution capabilities of the *Herschel Space Observatory* show that it is ubiquitous. Most importantly, star formation takes place within these filaments [2]. Figure 1 shows the column density map of a molecular cloud as well as the positions of young stellar objects. The stars are forming along the gravitationally unstable parts of the filaments, i.e. where the mass per unit length of the filament exceeds the critical value of $2c_s^2/G$ [2], where c_s is the sound speed of the gas and G is Newton's gravitational constant.

Several other physical processes also play important roles. While we do not examine magnetic fields in detail in this paper, they are observed within both the diffuse and molecular components and within star-forming gas. Magnetic fields in molecular gas have energy densities comparable to, but somewhat smaller than, that of gravity [3]. The strength of magnetic fields is measured by the ratio of the gravitational to magnetic energy densities, known as the 'mass to flux' ratio μ. Clouds and cores vary strongly in the value of μ, but typically have values $\mu \leq 5$, which has several important consequences. One of these concerns the radial structure of density filaments, which are observed to have a much shallower dependence on radius than models of purely hydrodynamic, self-gravitating filaments [4]. Good fits to the data are obtained for models of filaments that are wrapped with a helical magnetic field [5]. Such structures have been detected by submillimetre polarimetry observations [6]. The formation of massive stars results in a copious outpouring of energy and momentum in the form of radiation fields and outflows that are pumped into the surrounding gas through the action of shocks. Such 'feedback' effects play a profound role in shutting down star formation and in energizing the large-scale ISM.

Although several physical processes play a role in structuring molecular gas—including turbulence, gravity, magnetic fields and feedback due to stellar radiation and energetic protostellar outflows—the spectrum of stellar masses that results (known as the IMF) is rather simple and appears to be universal. The IMF is established at the scale at which star clusters are formed (a few parsecs). It has been described by several different functional forms, including a piecewise power law [7], a lognormal [8] and, more recently, a lognormal with a high-mass power law tail [9]. All the studies of the IMF show that stars more massive than $0.5M_\odot$ follow the famous Salpeter power-law form $dN \propto m^{-2.3}$.

There have been many theoretical attempts to explain the particular form of the IMF. For example, the lognormal distribution for the IMF at low masses could be due to gas supported by thermal pressure, whereas the Salpeter tail could be generated by the higher-mass cores that would be supported by turbulent pressure [10]. An alternative explanation is that an initial lognormal distribution develops a power-law tail as dense cores gradually accrete [11]. Elmegreen [12] remarked that, if all gas above a certain density threshold in a lognormal distribution can form stars, then it is possible to recover the well-known Schmidt law that governs the global star formation rate in galaxies (see also [13]).

The IMF must ultimately derive from the structure of the molecular gas. In this paper, we focus on the role that shocks and vorticity play in establishing the basic gas structure out of which the IMF ultimately arises. While turbulence has often been invoked as a theoretical framework, we
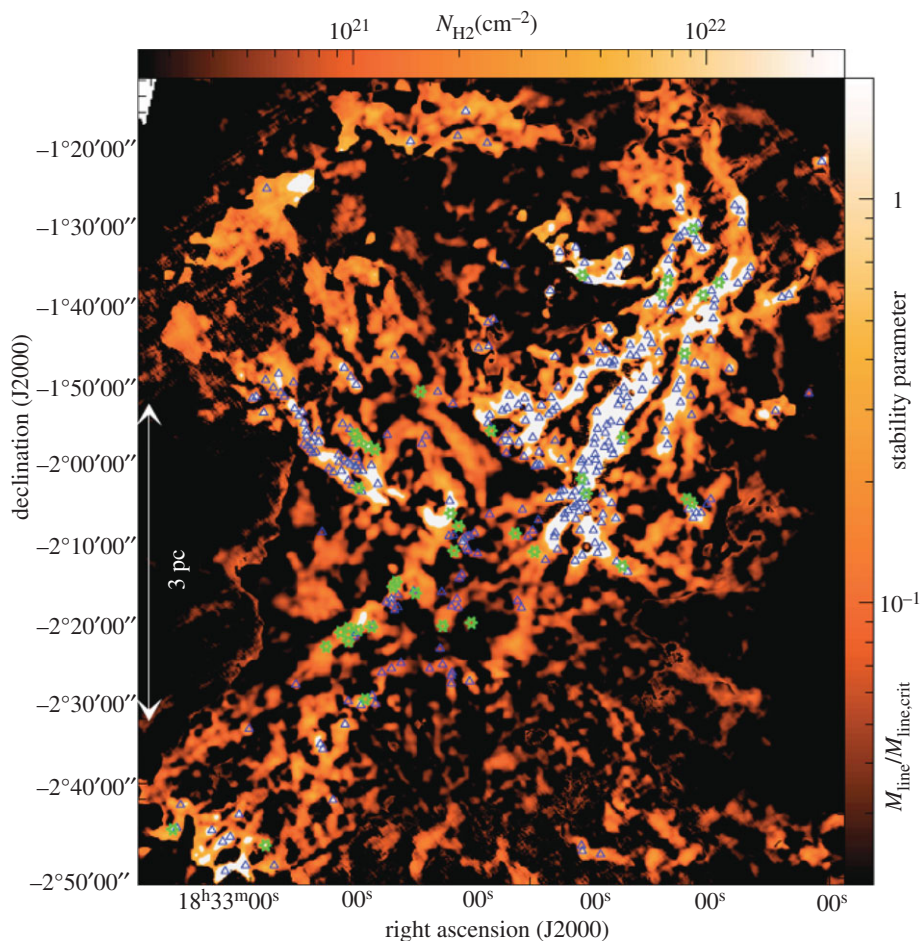
Figure 1. Column density map of the Polaris molecular cloud, derived from *Herschel Space Observatory* data. Adapted from [2].

show that the spatial, density and velocity structure of flows is much better understood in terms of the action of interacting shock waves. This has several important ramifications for the general structure of the IMF.

2. Understanding the observations of interstellar gas: supersonic turbulence versus shocks

Observations of chaotic, supersonic motions in interstellar gas have often been interpreted as arising from 'supersonic turbulence'. A basic property of turbulence is that it redistributes energy and density over many length scales. This process creates a strongly inhomogeneous flow, which, in the context of molecular clouds, produces some regions that are much denser than others. Sufficiently massive cores (greater than the local Jeans mass) will then collapse under their own gravity. This local collapse of dense cores begins the process of star formation. In addition to transferring energy and density over a wide range of length scales (determined by the Reynolds number of the flow), turbulence also makes an initially uniform density very inhomogeneous in space. This is because turbulence is extremely intermittent in space: the small-scale regions (and hence energy dissipation) are concentrated on a small subset of space.

The ISM, however, is more naturally pictured as a medium that is repeatedly lashed with shock waves that arise from a wide range of energetic astrophysical processes. Energy does not necessarily need to cascade from scale to scale: intersecting shocks and curved shocks can simultaneously excite energy over an enormous range of length scales. In addition, intersecting shocks and curved shocks efficiently generate vorticity. We investigate the observational constraints on these mechanisms below.

(a) Spatial structure and density fluctuations

On the largest galactic scales (several kpc), the overall structure of the shock-dominated, diffuse ISM of the Galaxy is seen in the neutral hydrogen (H I) gas observations such as the Canadian Galactic Plane Survey [14]. These 21 cm maps of radio emission show that the diffuse ISM is highly filamentary, and abounds in bubbles, cavities and channels carved out by radiation, winds and supernova explosions from massive stars. Most stars form in star clusters, and it is the massive stars within them that heat and ionize the surrounding molecular and atomic gas through their intense radiation fields. The feedback from radiation fields produces H II regions (ionized hydrogen) [15]. Towards the end of their short lives, massive stars produce stellar winds followed by supernova explosions. Recent estimates [16] based on the properties of the largest giant molecular clouds (GMCs) in the Galaxy indicate that the star formation efficiency in the Galaxy is very low, in the range $\epsilon_{GMC} \simeq 0.002$–$0.2$, with estimated star formation rates per free-fall time of the molecular cloud being near unity. The inference is that radiation pressure from massive stars in young star clusters forming in these large GMCs very efficiently destroys most of the molecular gas that is collapsing and attempting to form stars. Taken together, feedback processes disperse significant amounts of molecular gas, which probably accounts for the low star formation efficiency in galaxies. A similar structure of the ISM is also observed in our satellite dwarf galaxy, the Large Magellanic Cloud (LMC; see [17,18]). A bird's eye view of the relation between diffuse and molecular gas on the one hand, and the pattern of star formation and global density waves in a face-on disc galaxy on the other, is seen clearly in the Hubble Space Telescope image of M51. In this image, the filamentary distribution of dense dust lanes that are associated with the spiral pattern is obviously associated with the occurrence of young star clusters.

The prevalence of shock-driven processes extends down to the scales that characterize molecular clouds on tens of parsecs. One of the best-studied regions is the Orion molecular cloud. The large-scale structure of the Orion A and B clouds on 100 pc scales, mapped using an extinction technique [19], is clearly filamentary. The typical density of such gas is a few hundred cm^{-3}, which, though self-gravitating, is still too diffuse for star formation to occur. We can follow the filamentary structure down to 10 pc scales, wherein we see the famous integral filament, which was mapped at $850\,\mu m$ by the submillimetre observatory onboard the James Clerk Maxwell Telescope [20]. The dense star-forming gas in a molecular cloud occurs at 1 pc scales. The typical density for such a region is $10^5\,cm^{-3}$ and it is here that clusters of stars form. Individual embedded infrared objects—young stars in the process of formation—are seen in dense fluctuations known as cores, within such cluster-forming regions. Long-standing studies of the structure and physics of such cores [21] show that they have length scales of the order of 0.04 pc and smaller. Sufficiently low-mass cores have subsonic velocity dispersion [22]. The mass spectrum of cores has been analysed for a number of different clouds [23–26] and has been found to be very similar in form to that of the IMF. As an example, Alves *et al.* [27] showed in their extinction map of the Pipe nebula that the core mass function could be overlaid on the IMF by shifting the curve down in mass by a factor of three.

The structure and scaling of turbulence intermittency is a major outstanding problem in turbulence theory [28], although its existence is well established. Analysis of dust extinction maps [29] has shown that the probability density function (PDF) of column density for star-forming molecular cloud complexes is well described by a lognormal distribution, except at high densities, where the PDF follows a power law with slopes in the range from roughly -1.5 to

−4.2. The density distribution can be converted to a mass distribution (called the IMF) if a length scale is associated to each density. This can be done, for example, by assuming that the density fluctuations follow the same Kolmogorov scaling as the velocity, which seems to be the case. The resulting PDF still has the form of a lognormal distribution with a power-law tail at large masses. The peak of this IMF is a mass characteristic of gravitational collapse [10,30], whereas the power-law tail has a so-called Salpeter scaling exponent of about −1.35.

(b) Velocity structure and fluctuations

Let us now look at the velocity structure of gas over these many scales. The sparse gases and plasmas that fill interstellar space have velocity and mass density energy spectra characteristic of a neutral, incompressible fully developed turbulent fluid [31]. For example, radio observations of the diffuse ISM have found that density fluctuations follow a so-called 'big power law in the sky': Kolmogorov-like scaling $k^{-5/3}$ of the energy spectrum extends over 11 orders of magnitude, from 10^6 to 10^{17} m [32]! Chepurnov & Lazarian [33] have recently performed a very careful analysis to show that the data are indeed consistent with a single Kolmogorov spectrum over the full range of length scales. The ratio of the largest to smallest length scales increases like $Re^{3/4}$, where Re is the Reynolds number. Thus, these astrophysical flows must have an extremely high Reynolds number of about 10^{14}, making them the most turbulent flows known. Other fluctuations have power-law spectra with exponent $\alpha \in [-1.5, -2.6]$ [31], also suggestive of (possibly two-dimensional) turbulence. This is surprising because the ISM has a very large mean free path, is conducting, has an embedded magnetic field, and is strongly compressible. One would therefore expect the ISM to have very different dynamics from a simple Newtonian incompressible flow. The origin of the turbulence-like properties of the ISM over at least 11 orders of magnitude remains one of the central mysteries of astrophysical fluid dynamics.

Some attempts have been made to explain the observed Kolmogorov scaling in the context of a conducting, compressible fluid. A more comprehensive approach to incompressible magnetohydrodynamic (MHD) turbulence has emphasized the anisotropy that is stamped on the turbulence by the magnetic fields [34]. This gives an energy spectrum $k_\perp^{-5/3}$ in directions perpendicular to the mean magnetic field. However, the theory is not rigorous and it does not apply to the solar wind (which also exhibits a Kolmogorov scaling). Furthermore, other weak turbulence calculations find quite different scalings: $k_\perp^{-2}$ or $k_\perp^{-3/2}$. Stationary constant-flux solutions exhibit exponents anywhere in the range from −1 to −3 depending on the asymmetry of the forcing [35]. In addition, MHD turbulence is damped very quickly (in about one eddy turnover time). Therefore, any strongly turbulent flow would need a constant source of energy or would be unlikely to reach a stationary statistical state (characteristic of the so-called fully developed turbulence). In summary, there is still no convincing explanation of why the ISM density and velocity fluctuations should follow a single Kolmogorov inertial range scale over such a wide range of scales. We also note that recent high-resolution simulations of strongly magnetized MHD turbulence find a $k_\perp^{-3/2}$ scaling, rather than Kolmogorov $k_\perp^{-5/3}$ scaling. As suggested by Boldyrev et al. [36], this discrepancy could be due to scale-dependent dynamic alignment of the velocity and magnetic field vectors.

The Kolmogorov turbulence interpretation of the astrophysical data is also inconsistent with high-resolution simulations. As Johnsen et al. [37] point out in their comprehensive review of high-resolution methods for numerical simulations of compressible turbulence with shock waves, compressible turbulence is characterized by weak shock waves (eddy shocklets) that develop spontaneously from the turbulent fluctuations. Shocklets were first observed in the numerical simulations performed by Kida & Orszag [38]. These shocklets develop when the turbulence Mach number (based on the r.m.s. velocity) $M_t > 0.3$. Thus, even weakly compressible turbulence will be dominated by shocks and shock interactions. This suggests that compressible turbulence should have a energy exponent closer to −2, rather than the −5/3 predicted for incompressible turbulence. Indeed, this is what is seen in the high-resolution numerical simulations of Kritsuk et al. [39].

Both the velocity and magnetic fluctuations in solar winds also follow a Kolmogorov-like $-5/3$ turbulence scaling, despite the solar wind also being a conducting, compressible fluid [40]. This observation has usually been explained using a variation of Sridhar & Goldreich's [34] theory, although Borovsky [41] has cautioned that the $-5/3$ scaling could simply be due to discontinuities in the data, and may not actually be a signature of turbulence. We will explore the possibility that discontinuities (or other singularities), produced by shocks, might be the origin of the observed velocity and density scalings.

In summary, astrophysical fluctuations of density and velocity appear to have some of the characteristics of fully developed turbulence, although it is difficult to reconcile this interpretation with the actual physical properties of the ISM. In the following, we review the results of computer simulations addressing these questions.

3. Turbulence and fragmentation: simulations

Computer simulations have been the tool of choice in studies of turbulent flow and have provided some of the most important new insights into the link between shocks, supersonic turbulence and star formation in molecular clouds [42–44]. The role of 'turbulence' is central in this picture because it drives the formation of filamentary structure, produces the spectrum of dense cores, and can even account for the wide range of spins associated with these cores. While many simulations of structure formation drive, or impose an initial velocity spectrum on, the gas, the most basic question about astrophysical turbulence concerns the processes that actually drive it. In this section, we review the insights that simulations have given us into these processes over this wide range of scales.

On the scales of 10 kpc characterizing a disc galaxy, simulations of the effect of global spiral waves driven by a perturbing spiral potential have shown that the shock waves associated with these waves compress the gas into dense clouds, with an internal 'turbulent' velocity dispersion that can be associated with molecular clouds [45,46]. The diffuse ISM is also strongly influenced by the shocks, and the PDF of this component is well described by lognormal density PDF [13,47–49]. The large-scale shocks induce molecular cloud formation and create large velocity dispersion, i.e. turbulence. Simulations of the formation of GMCs have also idealized the process as the collision of supersonic streams of gas [50]. This work shows that, at that time when collision-induced turbulence is dominated by gravitational energy of the building clouds, clouds go into global gravitational collapse. As in combustion and pollution dispersion, turbulence is important in these processes for its extremely efficient mixing and large range of active length scales.

We have already noted that massive stars produced within sufficiently massive star clusters in GMCs provide strong feedback on their natal clouds and galactic environments. One mechanism that has been extensively simulated is the effect of multiple supernova explosions on interstellar gas. Massive stars drive three highly energetic phenomena into the surrounding gas: ionization fronts originating from the intense radiation fields of massive stars, a strong stellar wind and, in the end phase of their evolution, a supernova explosion. Simulations of supernova explosions in the Galactic disc show the highly textured medium and extreme density contrasts over six orders of magnitude in volume density ($10^{-4} < n < 10^2$ cm^{-3}) that arise from supernovae going off in a galactic disc [51].

As we descend to the scale of a molecular cloud, many studies have imposed driven or initial 'turbulent' velocity fields on gas within a periodic-box set-up and for which the source of the turbulence is not specified. The earliest results of such experiments [52] showed that lognormal density distributions were produced independent of whether the turbulence was driven at some wavenumber k or allowed to damp away (e.g. review [53]). As an example, Tilley & Pudritz [54] studied the combined effects of turbulence and self-gravity in a periodic-box simulation in which an initial velocity field (initially set to match a Kolmogorov or Burgers spectrum) was allowed to decay in a hydrodynamic simulation. By identifying regions that could be thought of as 'cloud cores', it was found that the mass function for such cores obeyed a lognormal distribution with a power-law tail at high masses. It is important to note that a wide variety of density fluctuations
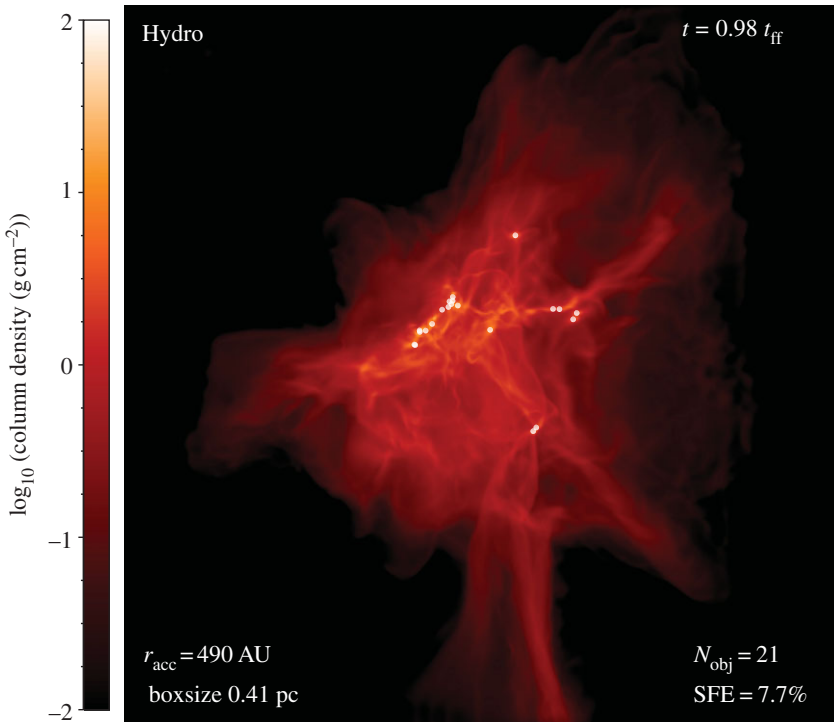
Figure 2. The formation of stars along filaments in a Flash adaptive mesh refinement simulation of a cluster-forming clump with $100 M_\odot$, about 100 Jeans masses and an initial scale of 0.4 pc. Adapted from Duffin *et al.* [57].

with core-like properties were identified in these simulations. Applying the virial theorem to these density fluctuations, it was found that a wide range of objects exist, a few of which are in equilibrium, but the bulk being either states that were bound or unbound. The surface pressure upon density fluctuations is an important contribution towards creating gravitationally bound cores. A large fraction of the lower-mass fluctuations tended to be gravitationally unbound, so that turbulence, rather than gravity, appears to dominate the dynamics of the lower-mass fluctuations.

Recent simulation shows that turbulence plus gravity can reproduce the observation of power-law tails in the column density PDFs of molecular clouds [55]. The initial conditions in this periodic-box simulation were prepared by applying an initial large-scale random force to the gas, which, after $4.8 t_{ff}$ free-fall times, was switched off while gravity and adaptive mesh refinement (AMR) of the grid was turned on. The adaptive refinement of the grid is necessary to follow the evolution of gravitating gas, because it is essential to resolve (by at least four grid cells) the local gravitational instability scale (the so-called Jeans length) sufficiently so that spurious mesh-induced fragmentation of the gas does not occur [56]. The experiments showed that an initial lognormal state was produced and that, with the onset of gravity, this lognormal distribution developed a power-law tail that extended over more than three orders of magnitude. The power-law slope for the tail of the column density was in the range $[-2.8, 2]$.

Figure 2 shows a snapshot of a simulation [57] of the formation of a small cluster within an initial $100 M_\odot$ star-forming clump of gas within a molecular cloud, containing about 100 initial Jeans masses, at a gas temperature of 10 K, with size of simulated region being 0.4 pc. Collapsing regions that give rise to stars are traced by sink particles. The simulation clearly shows that the star formation is tightly associated with the filaments. This evidence suggests that it is the gravitational instability along the filament that initiates the formation of the dense collapsing regions.

The formation of filaments in many of these simulations involves the oblique collisions of planar shock fronts that arise from the initial velocity field. The collision of two sheets (shock wave fronts) is a line. Thus, filaments represent the densest structures that supersonic turbulence, or, in our view, a collection of shock waves, can produce. It is therefore not surprising that dense cores would appear to form along filaments, as many simulations have shown. The formation of a filament by such a collision process is clearly seen in work by Banerjee *et al.* [58] where the collision of two quasi-planar shocks is seen to give rise to a density filament.

Another key aspect of the 'turbulent fragmentation' picture of structure formation is that it provides a natural explanation for the origin of angular momentum for cores, and hence for the origin of protostellar discs. Rotational energies are generally a small fraction of the gravitational energy of the system. The average value of the ratio of the rotational to gravitational energy is $\beta_{\rm rot} \simeq 0.01$, but its value spans several orders of magnitude: for both low-mass cores with a range 2×10^{-3} to 1.4 [59] and high-mass cores [60] in the range 4×10^{-4} to 7×10^{-2}. While rotational energy is thus too low to play a significant role in the dynamics of the cores, it is significant in establishing the initial conditions for the formation of protostellar discs on much smaller scales (a few to several hundred astronomical units, AU). Angular momentum can arise as a consequence of the oblique collision of shock waves [54,61]. The range of spins of such cores can be quite broad, extending over several orders of magnitude. In simulations by Banerjee *et al.* [58], the angular momentum of this gas arises from the fact that the filament is clearly associated with the intersection of two sheets, which are presumably the shock fronts that are generated from the initial supersonic velocity field set up for the cloud. The large-scale flow along the filament has sufficient angular momentum that an accretion disc is built up.

We now turn to discuss recent results [62] in which we showed that Kolmogorov scaling over many length scales and the observed skewed lognormal density PDF could arise from repeated shock interactions, without the need for fully developed turbulence. In addition, we discuss the physical origin of the angular momentum (i.e. vorticity) that is generated in interacting shocks as well as in curved shocks.

4. Shock forcing of turbulence

We have noted that the collision of shock waves generates filaments, and that the simulations typically and rapidly produce lognormal structure in the gas. In this section, we show that compressible turbulence fluctuations produce the lognormal part of the distribution through interaction of eddy shocklets. Thus, lognormal structure, which is evident in the IMF, has its roots in the basic dynamics of interacting shock waves. While gravity certainly can produce power-law tails observed in molecular cloud density PDFs, we show that feedback processes produce spherical shocks, which also give rise to power-law tails. The role of spherical shocks (or spherical expansion waves) has been confirmed in a recent numerical study [55].

(a) Regular intersection of planar shocks

The simplest type of shock interaction is the regular intersection of two plane shocks of unequal strength [63,64]. Figure 3*a* shows the basic features of such an interaction: both shocks are bent slightly, the flow is rotated and a vortex sheet (or slipstream) is generated downstream of the shock. As sketched in figure 3*b*, the vortex sheet is unstable and produces a sequence of vortices via the Kelvin–Helmholtz instability. These vortices in turn become unstable and generate three-dimensional turbulence via a secondary instability (note that the intersection of two plane shocks of equal strength will not generate a vortex sheet). As seen in the simulations described in the previous section, a dense filament is observed just behind the shock intersection point. One expects that the density further downstream of the shock should be much more homogeneous owing to the efficient turbulent mixing produced by the unstable vortex sheet. Note that two shocks generically intersect in a line, and this explains the fact that the most over-dense regions have a filamentary structure.
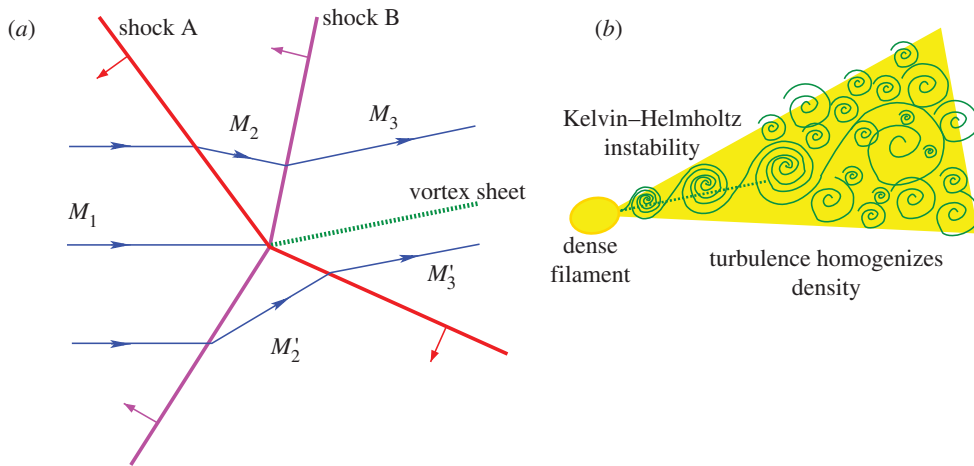
Figure 3. (a) Regular intersection of two plane shocks of unequal strength (the figure shows a two-dimensional section). M_1, M_2, M_2', M_3 and M_3' are the Mach numbers of the flow in the various regions. Note that the shocks are slightly bent, the streamlines are rotated and a vortex sheet is generated downstream of the shocks. (b) Instability of the vortex sheet produces turbulence that mixes and homogenizes the density away from the shock intersection point.

It is important to note that, as discussed below, a vortex sheet instantaneously distributes kinetic energy over all length scales and has a power-law energy spectrum $E(k) \sim k^{-2}$. This initial spectrum becomes shallower as the vortex sheet becomes unstable.

In summary, the regular intersection of two unequal planar shocks generates both a dense filamentary structure and turbulence (via the destabilization of the vortex sheet produced behind the shock intersection line). In the following section, we review how multiple shock passages may build up the lognormal density distribution and $k^{-5/3}$ energy spectrum observed in the ISM. These multiple shock passages may involve the intersecting plane shocks just discussed or individual self-focusing shocks.

(b) A shock mechanism for the density PDF and energy spectrum

Here, we review the shock-based mechanisms proposed in recent work by Kevlahan & Pudritz [62] to explain the lognormal PDF of density and turbulence-like $k^{-5/3}$ spectrum of kinetic energy observed in the ISM. We focus here on the role of individual curved shocks, but the intersecting plane shocks discussed in the previous section play a similar role.

Kevlahan [65] derived an expression for the vorticity jump across a shock wave that includes the effect of the upstream turbulence. If we assume that the turbulence is isentropic and quasi-steady (with respect to the passage time of the shock), then the vorticity jump in the binormal direction b is

$$\delta\boldsymbol{\omega} \cdot \boldsymbol{b} = \frac{\mu^2}{1+\mu} \frac{\partial M_s}{\partial S} + \frac{1}{M_s} \left(\frac{\mu}{1+\mu} M_s^2 - 1 \right) \left[\frac{\partial \frac{1}{2} M_t^2}{\partial S} + \boldsymbol{\omega} \times \boldsymbol{u} \cdot \boldsymbol{s} \right] + \mu\boldsymbol{\omega} \cdot \boldsymbol{b}, \tag{4.1}$$

where μ is the normalized density jump (i.e. the shock strength), M_s is the Mach number of the shock, $\partial/\partial S$ is the tangential part of the directional derivative, M_t is the turbulent Mach number of the upstream flow, and u and ω are the velocity and vorticity respectively of the upstream turbulence normalized by sound speed. Equation (4.1) may be simplified for strong shocks by using the approximation $\mu \approx 2/(\gamma - 1)$. The density jump is given by

$$\frac{\delta\rho}{\rho} \equiv \mu = \frac{M_s^2 - 1}{1 + 1/2(\gamma - 1)M_s^2}. \tag{4.2}$$

The first term on the right-hand side of (4.1) represents vorticity generation due to the variation of the shock speed M_s along the shock (e.g. due to shock curvature); by symmetry it is exactly zero for spherical and cylindrical shocks. The second term is baroclinic generation of vorticity due to misalignment of pressure and density gradients across the shock; and the final term is the jump in vorticity due to the conservation of angular momentum across the shock.

Because shocks are nonlinear waves (unlike acoustic waves), M_s is larger in regions of concave curvature and smaller in regions of convex curvature (with respect to the propagation direction of the shock). This difference in shock strength increases over time and eventually causes curved shocks to *focus* at regions of minimum curvature, developing a flat shock disc bounded by regions of very high curvature (often called kinks) [66]. This structure is called a Mach disc and generates vortex sheets downstream of the shock as in the case of intersecting plane shocks. The discontinuous shock strength at the kinks is called a shock–shock [67] and is essentially the same as the intersection line of a pair of intersecting plane shocks.

In the ISM, focusing of individual shocks could arise due to reflection off density gradients (e.g. vertically stratified structure in discs), density inhomogeneities or small variations in shock curvature in blast waves.

Because the first term on the right-hand side of (4.1) is approximately singular at the location of a kink, vortex sheets develop in the flow downstream of the kinks. These vortex sheets themselves have an energy spectrum $E(k) \sim k^{-2}$ and generate turbulence exponentially fast via the Kelvin–Helmholtz instability. Note that this produces a -2 spectrum in the downstream flow, even when the shock is no longer present. In other words, the -2 energy spectrum scaling could be the *trace* of a shock, rather than requiring the presence of a shock.

Kevlahan & Pudritz [62] showed for the first time how multiple passages of focused shocks could produce an energy spectrum shallower than -2. Previously, the relevance of multiple shock passages for astrophysical flows was established by Kornreich & Scalo [68], who found that the average time between shock passages in the ISM is 'small enough that the shock pump is capable of sustaining supersonic motions against readjustment and dissipation' [68, p. 366].

The energy spectrum of the three-dimensional flow after one, two and three passages of a focused shock with principal wavenumbers $k_1 = k_2 = 1$, $M_s = 6$ and zero velocity initial condition was analysed by Kevlahan & Pudritz [62]. The key result is that the initial k^{-2} scaling of the energy spectrum (due to the velocity discontinuity associated with the vortex sheet downstream of the shock–shocks) becomes gradually shallower with each shock passage. This redistribution of energy to smaller scales is due to the quadratic baroclinic terms depending on the (inhomogeneous) upstream flow in the vorticity jump equation (4.1). Although the effect is entirely kinematic, these quadratic terms redistribute energy among scales in a way analogous to the quadratic nonlinearity in the Navier–Stokes equations. After three shock passages, the energy spectrum has a scaling similar to $k^{-5/3}$. More shock passages would produce an even shallower power law. Moreover, the form of the energy spectrum is relatively insensitive to the choice of initial condition.

Simulations have suggested previously that the structure observed in the ISM and molecular clouds probably derives from shock-driven processes. The results presented above from Kevlahan & Pudritz [62] give an alternative explanation of the energy spectrum scalings close to $-5/3$ observed in astrophysical fluctuations. They also suggest why the spectrum is shallower than the scaling -2 expected for compressible turbulence (due to the eddy shocklets generated spontaneously in strongly compressible flows). The observed $E(k) \approx k^{-5/3}$ 'big power law in the sky' may be due primarily to kinematic effects associated with repeated shock passages, and may not in fact require fully developed turbulence. This could also explain why the power law extends over such a huge range of length scales (spanning several different physical regimes, from the diffuse ISM to molecular gas), because the power law of a shock-driven flow is due to a singularity, and so extends over all scales (until the viscous cut-off).

We have shown that interacting shocks generate a lognormal distribution of density. As mentioned above, compressible turbulent flows with $M_t > 0.3$ spontaneously generate small, relatively weak and highly curved shocks, called 'eddy shocklets' [38]. It is therefore likely that
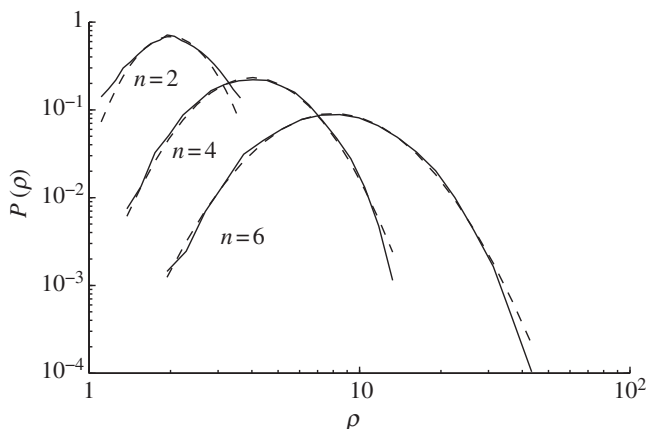
Figure 4. Convergence to a lognormal PDF of density after $n = 2, 4, 6$ shock passages. Dashed line denotes lognormal distribution; solid line denotes PDF of density. Adapted from Kevlahan & Pudritz [62].

a particular region of space is hit multiple times by eddy shocklets of varying strengths. If we now assume that the density does not change significantly between shock passages (i.e. that the density changes are primarily due to shock compression), then from equation (4.2) the density after n shock passages is

$$\rho^{(n)}(x) = \prod_{j=0}^{n}(1 + \mu^{(j)}(x)), \qquad (4.3)$$

where the density is normalized in terms of the initial uniform density ρ_0. We now treat the shock strengths $\mu^{(j)}(x)$ as identically distributed random variables. Then, because $(1 + \mu^{(j)}(x)) > 0$ we can take the logarithm of both sides and apply the central limit theorem to the resulting sum. This shows that the logarithm of density is normally distributed, i.e. the density PDF follows a lognormal distribution,

$$P(\rho) = \frac{1}{\sqrt{2\pi}\sigma\rho} \exp\left(-\frac{(\log(\rho) - \overline{\log\rho})^2}{2\sigma^2}\right). \qquad (4.4)$$

Note that application of the central limit theorem to derive (4.4) requires only that the random variables $\log(1 + \mu^{(j)}(x))$ have finite mean and variance [69].

Kevlahan & Pudritz [62] pointed out that the convergence to the lognormal distribution is very rapid. Figure 4 (reproduced from Kevlahan & Pudritz [62]) shows that as few as three or four shock passages generate a very good approximation to the lognormal distribution. This explanation is consistent with observations from experiments that the lognormal distribution of density develops very quickly, and seems to be associated with the first shock interactions [70]. Thus, the lognormal distribution should develop well before self-gravity becomes important. In fact, as proposed below, the denser cores associated with the lognormal distribution are probably the catalysts for the self-gravity-driven collapse that produces the power-law tail at high densities.

(c) Feedback effects and power-law tails

As first suggested in Kevlahan & Pudritz [62], a power-law tail of the density distribution can be produced by spherical shock waves that interact with a pre-existing lognormal distribution. These shocks could be due to blast waves or stellar wind (once the first stars have formed), or could take the form of an expansion wave generated by a rapidly collapsing core (as suggested by Kritsuk et al. [55]). The origin of the shock wave will change the power-law scaling, but it is the spherical symmetry of the shock that produces a power-law scaling at large densities.

Following Kevlahan & Pudritz [62], we assume a blast wave solution for strong spherical shocks. Dokuchaev [71] generalized the Sedov–Taylor self-similar blast wave solution to the sustained energy injection case $E(t) \propto t^p$. Here $p = 0$ corresponds to an instant shock (e.g. such as a supernova), whereas $p = 1$ corresponds to continuous energy input (i.e. a stellar wind).

As in the previous case, we take a probabilistic view and assume that the PDF of finding a particular value of gas density ρ_1 is proportional to the space–time volume where the density exceeds ρ_1,

$$P(\rho > \rho_1) \propto \int_0^{t(\rho_1)} R^3(t)\,dt, \tag{4.5}$$

where $R(t) \propto t^{(2+p)/5}$ is the radius of the spherical shock at time t and $t(\rho_1)$ is the time at which the density behind the shock is equal to ρ_1. Using the relation $M_s(t) \propto R(t)/t$, equation (4.2) can be inverted to find $t(\rho_1) \propto \rho^{5/2(-3+p))}$.

Using the definition of the PDF, we find that the PDF of density due to the interaction of a homogeneous gas with a spherical blast wave has the form

$$P(\rho) = \frac{d}{d\rho} \int_0^{t(\rho)} R^3(t)\,dt \propto \rho^{-(17+p)/(6-2p)} \tag{4.6}$$

(where we have relabelled ρ_1 as ρ). Therefore, the density PDF is a power law with exponent $-17/6 \approx -2.8$ for an instant shock and $-9/2 = -4.5$ for an injection shock. These slopes are significantly steeper than the Salpeter value for the mass PDF of -1.35. However, the actual relation between the density PDF and the mass PDF depends on the precise assumptions made about the scaling of clumps (i.e. mass equals density times a length scale cubed). Thus, one should not necessarily expect the same index for both the density and mass PDFs (although the power-law form should be robust). Furthermore, as mentioned earlier, analysis of dust extinction maps [29] gave scalings for the power-law tail of the density PDF of -1.5 to -4.2, roughly consistent with the spherical shock model.

It is important to note that observations measure PDFs of *column density* (i.e. density integrated along a line of sight), rather than PDFs of density itself. If there are many randomly distributed spherical shocks, then these two measures should be similar. However, if there is only one infinitely large spherical shock, the resulting density would have to be integrated to give a column density as in [55]. If the density is given by $\rho \sim r^{-n}$, then the column density is

$$2 \int_0^\infty \rho\left(\sqrt{R^2 + x^2}\right)\,dx \propto R^{1-n}, \tag{4.7}$$

which also has a power-law PDF, but with slope $-2/(n-1)$. In the blast wave model, $\rho \sim r^{-2(3-p)/(2+p)}$ and thus $n = 3$ for a blast wave and $n = 4/3$ for an injection shock. Thus, if we assume a single blast wave, the column density would scale like -1; whereas for the injection shock, the column density would scale like -6. Kritsuk *et al.* [55] found column density scalings for self-similar gravitational collapse of $-2, -2.8$ and -4, depending on the model. It therefore seems more likely that the observed power law is due either to expansion shock waves produced by self-gravitational collapse or to a collection of spherical blast waves. However, as noted below, the probabilistic interpretation helps explain the hybrid form of the PDF (both lognormal and power law).

Finally, we can find the PDF of density resulting from the interaction of a spherical shock with a lognormally distributed density field as the convolution of the PDF (4.6) with the lognormal distribution of density (4.4). This produces a PDF that is lognormal for small densities, and has a power law $\rho^{-(17+p)/(6-2p)}$ for high densities up to a maximum density proportional to $1/(\gamma - 1)$. Figure 5 (reproduced from Kevlahan & Pudritz [62]) shows the resulting hybrid PDF. If no more spherical shocks are generated, the distribution will slowly revert to a simple lognormal form. Thus, one expects that a power-law tail is a signature of a star-producing region, where shocks are produced either by intense stellar winds or by spherical expansion waves associated with self-gravitational collapse. The remaining question is whether such shock waves are able to account for so many decades of gas compression as can gravity.
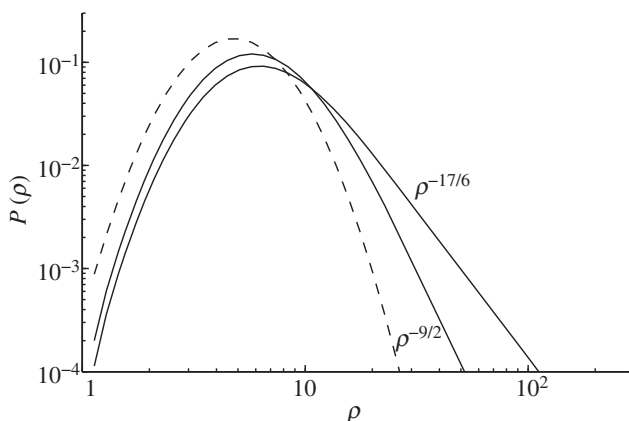
Figure 5. Generation of a power-law PDF at large densities in a nearly isothermal gas by a spherical blast wave interacting with a lognormally distributed density field. Dashed line is the initial lognormal PDF and the slopes $-17/6$ and $-9/2$ correspond to an instant shock and an injection shock, respectively. Note that the upper limit of the power-law range is proportional to $1/(\gamma - 1)$, and thus we expect the largest power-law ranges for nearly isothermal gases, i.e. those with $\gamma \approx 1$. Adapted from Kevlahan & Pudritz [62].

5. Conclusion

The structure of interstellar gas in general, and star-forming molecular clouds in particular, is shaped to a very important degree by interacting shock waves. Using two basic shock models (intersecting plane shocks and self-focusing curved shocks), we have shown that this provides a more self-consistent picture of the ISM and the conditions leading to star formation than traditional ideas of 'supersonic turbulence'. The lognormal aspect of the gas density is imprinted on the structure of the IMF of stars. The power-law tail at high masses can be produced by several mechanisms, certainly by gravity, but also by the shock waves resulting from radiative feedback processes during star formation. The generality of this behaviour of shock waves gives considerable support for the idea that, despite the complexity in the detailed physics, the structure and possible universality of the form of the kinetic energy spectrum and IMF are an expression of the physics of shock waves in gravitating media.

References

1. Schneider S, Elmegreen BG. 1979 A catalog of dark globular filaments. *Astrophys. J. Suppl. Ser.* **41**, 87–95. (doi:10.1086/190609)
2. André P. *et al.* 2010 From filamentary clouds to prestellar cores to the stellar IMF: initial highlights from the *Herschel* Gould Belt Survey. *Astron. Astrophys.* **518**, L102. (doi:10.1051/0004-6361/201014666)
3. Crutcher RM, Wandelt B, Heiles C, Falgarone E, Troland TH. 2010 Magnetic fields in interstellar clouds from Zeeman observations: inference of total field strengths by Bayesian analysis. *Astrophys. J.* **725**, 466–479. (doi:10.1088/0004-637X/725/1/466)
4. Ostriker J. 1964 The equilibrium of polytropic and isothermal cylinders. *Astrophys. J.* **140**, 1056. (doi:10.1086/148005)
5. Fiege JD, Pudritz RE. 2000 Helical fields and filamentary molecular clouds: I. *Mon. Not. R. Astron. Soc.* **311**, 85–104. (doi:10.1046/j.1365-8711.2000.03066.x)

6. Matthews BC, Wilson CD, Fiege JD. 2001 Magnetic fields in star-forming molecular clouds. II. The depolarization effect in the OMC-3 filament of Orion A. *Astrophys. J.* **562**, 400–423. (doi:10.1086/323375)

7. Kroupa P. 2002 The initial mass function of stars: evidence for uniformity in variable systems. *Science* **295**, 82–91. (doi:10.1126/science.1067524)

8. Miller GE, Scalo JM. 1979 The initial mass function and stellar birthrate in the solar neighborhood. *Astrophys. J. Suppl. Ser.* **41**, 513–547. (doi:10.1086/190629)

9. Chabrier G. 2003 Galactic stellar and substellar initial mass function. *Publ. Astron. Soc. Pac.* **115**, 763–795. (doi:10.1086/376392)

10. Hennebelle P, Chabrier G. 2008 Analytical theory for the initial mass function: CO clumps and prestellar cores. *Astrophys. J.* **684**, 395–410. (doi:10.1086/589916)

11. Basu S, Jones CE. 2004 On the power-law tail in the mass function of protostellar condensations and stars. *Mon. Not. R. Astron. Soc.* **347**, L47–L51. (doi:10.1111/j.1365-2966.2004.07405.x)

12. Elmegreen BG. 2002 Star formation from galaxies to globules. *Astrophys. J.* **577**, 206–220. (doi:10.1086/342177)

13. Wada K, Norman CA. 2007 Density structure of the interstellar medium and the star formation rate in galactic disks. *Astrophys. J.* **660**, 276–287. (doi:10.1086/513002)

14. Taylor AR *et al.* 2003 The Canadian Galactic Plane Survey. *Astron. J.* **125**, 3145–3164. (doi:10.1086/375301)

15. Peters T, Banerjee R, Klessen RS, Mac Low MM, Galván-Madrid R, Keto ER. 2010 H II regions: witnesses to massive star formation. *Astrophys. J.* **711**, 1017–1028. (doi:10.1088/0004-637X/711/2/1017)

16. Murray N. 2011 Star formation efficiencies and lifetimes of giant molecular clouds in the Milky Way. *Astrophys. J.* **729**, 133–147. (doi:10.1088/0004-637X/729/2/133)

17. Elmegreen BG, Kim S, Staveley-Smith L. 2001 A fractal analysis of the H I emission from the Large Magellanic Cloud. *Astrophys. J.* **548**, 749–769. (doi:10.1086/319021)

18. Meixner M, *et al.* 2006 *Spitzer* survey of the Large Magellanic Cloud: Surveying the Agents of a Galaxy's Evolution (SAGE). I. Overview and initial results. *Astron. J.* **132**, 2268–2288. (doi:10.1086/508185)

19. Cambrésy L. 1999 Mapping of the extinction in giant molecular clouds using optical star counts. *Astron. Astrophys.* **345**, 965–976. See http://aa.springer.de/papers/9345003/2300965.pdf.

20. Johnstone D, Bally J. 2006 Large-area mapping at 850 μm. V. Analysis of the clump distribution in the Orion A South molecular cloud. *Astrophys. J.* **653**, 383–397. (doi:10.1086/508852)

21. Jijina J, Myers PC, Adams FC. 1999 Dense cores mapped in ammonia: a database. *Astrophys. J.* **125**, 161–236. (doi:10.1086/313268)

22. Pineda JE *et al.* 2010 Direct observation of a sharp transition to coherence in dense cores. *Astrophys. J.* **712**, L116–L121. (doi:10.1088/2041-8205/712/1/L116)

23. Motte F, André P, Ward-Thompson D, Bontemps S. 2001 A SCUBA survey of the NGC 2068/2071 protoclusters. *Astron. Astrophys.* **372**, L41–L44. (doi:10.1051/0004-6361:20010543)

24. Johnstone D, Fich M, Mitchell GF, Moriarty-Schieven G. 2001 Large area mapping at 850 microns. III. Analysis of the clump distribution in the Orion B molecular cloud. *Astrophys. J.* **559**, 307–317. (doi:10.1086/322323)

25. Nutter D, Ward-Thompson D. 2007 A SCUBA survey of Orion: the low-mass end of the core mass function. *Mon. Not. R. Astron. Soc.* **374**, 1413–1420. (doi:10.1111/j.1365-2966.2006.11246.x)

26. Enoch ML, Evans NJ II, Sargent AI, Glenn J, Rosolowsky E, Myers P. 2008 The mass distribution and lifetime of prestellar cores in Perseus, Serpens, and Ophiuchus. *Astrophys. J.* **684**, 1240–1259. (doi:10.1086/589963)

27. Alves J, Lombardi M, Lada CJ. 2007 The mass function of dense molecular cores and the origin of the IMF. *Astron. Astrophys.* **462**, L17–L21. (doi:10.1051/0004-6361:20066389)

28. Alam J, Kevlahan NKR, Vasilyev OV. 2007 Scaling of space–time modes with Reynolds number in two-dimensional turbulence. *J. Fluid Mech.* **570**, 217–226. (doi:10.1017/S0022112006003168)

29. Kainulainen J, Beuther H, Henning T, Plume R. 2009 Probing the evolution of molecular cloud structure. From quiescence to birth. *Astron. Astrophys.* **508**, L35–L38. (doi:10.1051/0004-6361/200913605)

30. Padoan P, Nordlund A. 2002 The stellar initial mass function from turbulent fragmentation. *Astrophys. J.* **576**, 870–879. (doi:10.1086/341790)

31. Elmegreen BG, Scalo J. 2004 Interstellar turbulence I: observations and processes. *Annu. Rev. Astron. Astrophys.* **42**, 211–273. (doi:10.1146/annurev.astro.41.011802.094859)

32. Spangler SR. 1999 Interstellar turbulence: what radio astronomers can tell plasma theorists. In *Proc. Int. Conf. on Plasma Turbulence and Energetic Particles in Astrophysics, Cracow, Poland, 5–10 September 1999* (eds M Ostrowski, R Schlickeiser), pp. 1–4. See http://adsabs.harvard.edu/abs/1999ptep.proc....1S.

33. Chepurnov A, Lazarian A. 2010 Extending the big power law in the sky with turbulence spectra from Wisconsin Hα Mapper data. *Astrophys. J.* **710**, 853–858. (doi:10.1088/0004-637X/710/1/853)

34. Sridhar S, Goldreich P. 1994 Toward a theory of interstellar turbulence. 1. Weak Alfvenic turbulence. *Astrophys. J.* **432**, 612–621. (doi:10.1086/174600)

35. Galtier S, Nazarenko SV, Newell AC, Pouquet A. 2002 Anisotropic turbulence of shear–Alfvén waves. *Astrophys. J.* **564**, L49–L52. (doi:10.1086/338791)

36. Boldyrev S, Mason J, Cattaneo F. 2009 Dynamic alignment and exact scaling laws in magnetohydrodyamic turbulence. *Astrophys. J. Lett.* **699**, L39–L42. (doi:10.1088/0004-637X/699/1/L39)

37. Johnsen E *et al.* 2010 Assessment of high-resolution methods for numerical simulations of compressible turbulence with shock waves. *J. Comput. Phys.* **229**, 1213–1237. (doi:10.1016/j.jcp.2009.10.028)

38. Kida S, Orszag SA. 1990 Enstrophy budget in decaying compressible turbulence. *J. Sci. Comput.* **5**, 1–34. (doi:10.1007/BF01063424)

39. Kritsuk AG, Norman ML, Padoan P, Wagner R. 2007 The statistics of supersonic isothermal turbulence. *Astrophys J.* **665**, 416–431. (doi:10.1086/519443)

40. Roberts DA. 2010 Evolution of the spectrum of solar wind velocity fluctuations from 0.3 to 5 AU. *J. Geophys. Res.* **115**, A12101. (doi:10.1029/2009JA015120)

41. Borovsky JE. 2010 Contribution of strong discontinuities to the power spectrum of the solar wind. *Phys. Rev. Lett.* **105**, 111102. (doi:10.1103/PhysRevLett.105.111102)

42. Vazquez-Semadeni E, Passot T, Pouquet A. 1995 A turbulent model for the interstellar medium. 1: threshold star formation and self-gravity. *Astrophys. J.* **441**, 702–725. (doi:10.1086/175393)

43. Padoan P, Juvela M, Goodman AA, Nordlund Å. 2001 The turbulent shock origin of proto-stellar cores. *Astrophys. J.* **553**, 227–234. (doi:10.1086/320636)

44. Bonnell IA, Bate MR, Vine SG. 2003 The hierarchical formation of a stellar cluster. *Mon. Not. R. Astron. Soc.* **343**, 413–418. (doi:10.1046/j.1365-8711.2003.06687.x)

45. Bonnell IA, Dobbs CL, Robitaille TP, Pringle JE. 2006 Spiral shocks, triggering of star formation and the velocity dispersion in giant molecular clouds. *Mon. Not. R. Astron. Soc.* **365**, 37–45. (doi:10.1111/j.1365-2966.2005.09657.x)

46. Dobbs CL, Bonnell IA, Pringle JE. 2006 The formation of molecular clouds in spiral galaxies. *Mon. Not. R. Astron. Soc.* **371**, 1663–1674. (doi:10.1111/j.1365-2966.2006.10794.x)

47. Wada K, Norman CA. 2001 Numerical models of the multiphase interstellar matter with stellar energy feedback on a galactic scale. *Astrophys. J.* **547**, 172–186. (doi:10.1086/318344)

48. Tasker EJ, Bryan GL. 2008 The effect of the interstellar medium model on star formation properties in galactic disks. In *Formation and evolution of galaxy disks* (eds JG Funes, EM Corsini). Astron. Soc. Pac. Conf. Ser., vol. 396, p. 105. San Francisco, CA: Astronomical Society of the Pacific. See http://www.aspbooks.org/a/volumes/article_details/?paper_id=29311.

49. Tasker EJ. 2011 Star formation in disk galaxies. II. The effect of star formation and photoelectric heating on the formation and evolution of giant molecular clouds. *Astrophys. J.* **730**, 11. (doi:10.1088/0004-637X/730/1/11)

50. Vázquez-Semadeni E, Gómez GC, Jappsen AK, Ballesteros-Paredes J, González RF, Klessen RS. 2007 Molecular cloud evolution. II. From cloud formation to the early stages of star formation in decaying conditions. *Astrophys. J.* **657**, 870–883. (doi:10.1086/510771)

51. de Avillez MA, Breitschwerdt D. 2004 Volume filling factors of the ISM phases in star forming galaxies. I. The role of the disk–halo interaction. *Astron. Astrophys.* **425**, 899–911. (doi:10.1051/0004-6361:200400025)

52. Klessen RS. 2001 The formation of stellar clusters: mass spectra from turbulent molecular cloud fragmentation. *Astrophys. J.* **556**, 837–846. (doi:10.1086/321626)

53. Mac Low MM, Klessen RS. 2004 Control of star formation by supersonic turbulence. *Rev. Mod. Phys.* **76**, 125–194. (doi:10.1103/RevModPhys.76.125)

54. Tilley DA, Pudritz RE. 2004 The formation of star clusters. I. Three-dimensional simulations of hydrodynamic turbulence. *Mon. Not. R. Astron. Soc.* **353**, 769–788. (doi:10.1111/j.1365-2966.2004.08077.x)

55. Kritsuk AG, Norman ML, Wagner R. 2011 On the density distribution in star-forming interstellar clouds. *Astrophys. J.* **727**, L20. (doi:10.1088/2041-8205/727/1/L20)

56. Truelove JK, Klein RI, McKee CF, Holliman JH II, Howell LH, Greenough JA. 1997 The Jeans condition: a new constraint on spatial resolution in simulations of isothermal self-gravitational hydrodynamics. *Astrophys. J.* **489**, L179. (doi:10.1086/310975)

57. Duffin DF, Federrath C, Pudritz RE, Banerjee R, Klessen R. 2013 In preparation.

58. Banerjee R, Pudritz RE, Anderson DW. 2006 Supersonic turbulence, filamentary accretion and the rapid assembly of massive stars and discs. *Mon. Not. R. Astron. Soc.* **373**, 1091–1106. (doi:10.1111/j.1365-2966.2006.11089.x)

59. Goodman AA, Benson PJ, Fuller GA, Myers PC. 1993 Dense cores in dark clouds. VIII: velocity gradients. *Astrophys. J.* **406**, 528–547. (doi:10.1086/172465)

60. Pirogov L, Zinchenko I, Caselli P, Johansson LEB, Myers PC. 2003 $N_2H^+(1–0)$ survey of massive molecular cloud cores. *Astron. Astrophys.* **405**, 639–654. (doi:10.1051/0004-6361:20030659)

61. Jappsen A, Klessen RS. 2004 Protostellar angular momentum evolution during gravoturbulent fragmentation. *Astron. Astrophys.* **423**, 1–12. (doi:10.1051/0004-6361:20040220)

62. Kevlahan N, Pudritz RE. 2009 Shock-generated vorticity in the interstellar medium and the origin of the stellar initial mass function. *Astrophys. J.* **702**, 39–49. (doi:10.1088/0004-637X/702/1/39)

63. Liepmann HW, Roshko A. 1957 *Elements of gas dynamics*. London, UK: John Wiley & Sons.

64. Chapman CJ. 2000 *High speed flow*. Cambridge, UK: Cambridge University Press.

65. Kevlahan NKR. 1997 The vorticity jump across a shock in a non-uniform flow. *J. Fluid Mech.* **341**, 371–384. (doi:10.1017/S0022112097005752)

66. Kevlahan NKR. 1996 The propagation of weak shocks in non-uniform flows. *J. Fluid Mech.* **327**, 161–197. (doi:10.1017/S0022112096008506)

67. Whitham GB. 1974 *Linear and nonlinear waves*. London, UK: John Wiley & Sons.

68. Kornreich P, Scalo J. 2000 The galactic shock pump: a source of supersonic internal motions in the cool interstellar medium. *Astrophys. J.* **531**, 366–383. (doi:10.1086/308425)

69. Vazquez-Semadeni E. 1994 Hierarchical structure in nearly pressureless flows as a consequence of self-similar statistics. *Astrophys. J.* **423**, 681. (doi:10.1086/173847)

70. Nordlund ÅK, Padoan P. 1999 The density PDFs of supersonic random flows. In *Interstellar Turbulence, Proc. 2nd Guillermo Haro Conf.* (eds J Franco, A Carraminana). Cambridge Contemporary Astrophysics, pp. 218–222. Cambridge, UK: Cambridge University Press. (doi:10.1017/CBO9780511564666.034)

71. Dokuchaev VI. 2002 Self-similar spherical shock solution with sustained energy injection. *Astron. Astrophys.* **395**, 1023–1029. (doi:10.1051/0004-6361:20021305)